A Biomechanical evaluation of Patient-specific Flanged Acetabular Components: A Computational Model

Louise O'Connor, Friedrich Boettner, Jason Blevins, Jose Rodriguez, Joseph Lipman, Fernando Quevedo González, Mathias P. Bostrom, Timothy Wright, Peter Sculco, Hospital for Special Surgery, New York, NY
oconnorl@hss.edu

Disclosures: LOC (N), FB (1-OrthoDevelopment, Smith & Nephew; 3B-OrthoDevelopment, Smith & Nephew; 4-AccuJoint Inc.; 8-OrthoForum GmbH), JB (3B-Globus Medical, KCI, LimaCorporate), JR (1-ConforMIS, Exactech, Inc., Medacta, Smith & Nephew; 3B-ConforMIS, Exactech, Inc., Medacta, Smith & Nephew; 4-Tracpatch; 5-DePuy, Exactech, Inc., Smith & Nephew; 8-Clinical Orthopaedics and Related Research, HSS Journal, Journal of Arthroplasty; 9-American Association of Hip and Knee Surgeons, Eastern Orthopaedic Association), JL (7B: Exactech, Enovis, OrthoDevelopment; 3C: Extremity Medical), FQG (1-Lima Corporate,), MB (1-Smith & Nephew; 3B-Smith & Nephew; 5-Ines Mandl Research Foundation, Smith & Nephew; 8-Journal of Orthopaedic Research; 9-American Austrian Foundation, Hip Society) TW (7B: Exactech, Enovis, Mathys; 5: Enovis, Zimmer Biomet; 8: AJRR, OREF, Knee Society, Lima), PS (3B: Depuy, Intellijoint, EOS, Enovis, Zimmer Biomet; 4: Intellijoint, Parvizi Surgical Innovation; 5: Intellijoint)

INTRODUCTION: Patient-specific flanged acetabular components (FACs) are utilized to treat failed total hip arthroplasties (THAs) with large acetabular defects. FACs consist of a hemispherical cup within the defect and rigid flanges that span the ilium, ischium, and occasionally the pubis, and are fixed to the bone with multiple screws. A previous study from our institution developed a computational finite element (FE) model to quantify how hip center location affects the strain distributions in the implant and surrounding pelvic bone and the micromotions between implant and bone [1]. For this study an idealized case was modeled of a defect type that commonly requires FAC reconstruction – a superior-medial bone defect with bone loss in the anterior wall and acetabular rim. We then designed a patient-specific FAC to address this simulated bone defect and ran a computational model using FE software.
Our present study goal is to develop two FE models from real patient cases and perform a comparative study with the 'idealized' model previously computed.

METHODS: We selected two patient cases with available pre-revision CT scans without metal artifacts. We segmented and exported 3D geometries of the pelvis from each scan and exported the associated Hounsfield unit (HU) values. Since the two cases were performed and designed at HSS we had access to the original STL files of the implant which we exported into CAD software along with the pelvis, screws, and liner components. Each assembly was aligned according to Bergmann's coordinate system and subsequently exported into FE software (Abaqus, Dassault Systems) to generate two patient-specific computational models. Based on data from OrthoLoad and a free body diagram of the pelvis, we applied the predicted maximum hip contact force and corresponding abductor force during level gait. We also defined fixed boundary conditions at the pubic symphysis joint and the sacroiliac joint. To assign material properties to the bone we implemented a MATLAB code using the exported HU data from the CT scans. The material properties and resulting strains and micromotions were compared to the previously computed idealized model.

RESULTS: The geometry and bone density values assigned in the current models were derived directly from patient-specific CT data, ensuring a more physiologically accurate representation of bone quality. In contrast, the idealized model obtained material properties from a representative total hip arthroplasty (THA) patient, not a revision FAC patient. The resulting density distribution closely reflected the expected variation between cortical and cancellous regions, confirming that the CT-based assignment produced realistic bone density distributions. The distribution and magnitude of strain in the modified models were comparable to those of the original model, with strain values largely remaining within the range of ±0.003 (Fig. 1). Predicted micromotions also followed similar patterns and directions relative to the applied loads.

DISCUSSION: The findings indicate that patient-specific modeling produced mechanical responses comparable to those of the previously developed idealized model. The similarity in strain and micromotion patterns suggests that the overall mechanical behavior of the flanged acetabular component is governed primarily by implant geometry and loading configurations. However, the CT-based material mapping introduced a physiologically realistic representation of the bone, capturing regional variations in cortical and cancellous density. This enhancement improves the model's anatomical accuracy and provides a more accurate basis for simulations assessing implant fixation. The comparable mechanical results also suggest that the idealized model remains valid for general parametric studies, while patient-specific models are better suited for case-specific preoperative planning and validation of computational reconstruction strategies

SIGNIFICANCE/CLINICAL RELEVANCE: Our results show that the model can explore clinical and implant design variables known to influence the success of complex acetabular reconstruction using an FAC. By developing models based on real clinical cases we aim to design a patient-specific computational tool to determine an operative plan that will maximize the likelihood of long-term clinical and biomechanical performance for patients undergoing complex revision THAs with FACs. This framework could also be used to develop a biomechanically-based acetabular bone loss classification system to guide the development of patient-specific implants in the treatment of large acetabular bone defects. Our goal is to increase our number of patient cases and develop additional models following a standardized protocol.

REFERENCES: [1] Lee HY, et al. J Orthop Res. 2024;42:2228-2236

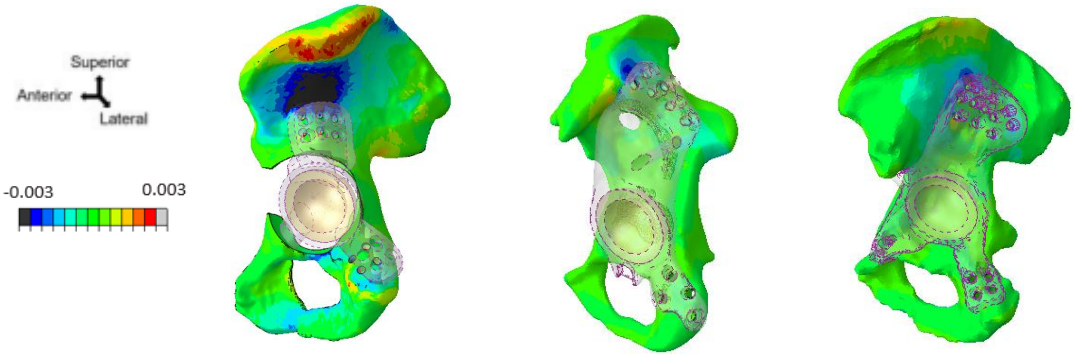

Fig 1: Strain distributions in the idealized model and patient cases 1 and 2